

Stabilizing chaotic dynamical system reproduction in reservoir computing

Satoshi Oishi^{1*}, Hiroshi Yamashita¹, Hideyuki Suzuki¹,
Sho Shirasaka¹

^{1*}Graduate school of information science and technology, The
University of Osaka, 1-5 Yamadaoka, Suita, 565-0871, Osaka, Japan.

Abstract

Reservoir Computing (RC), a type of recurrent random neural network, is a powerful framework for modeling complex and chaotic dynamics. However, its autonomous (closed-loop) operation is often plagued by inherent instability. Moreover, performance is highly sensitive to the reservoir’s random initialization, leading to vulnerability to noise and/or behaviour that bears no resemblance whatsoever to the target dynamical system. Here we identify a primary cause of this unreliability: the emergence of excessive, spurious unstable or neutral modes in the closed-loop dynamics. We introduce a simple deterministic input layer design principle that directly addresses this vulnerability by structurally suppressing the emergence of these spurious modes a priori (before training). Our approach dramatically improves robustness to both initialization sensitivity and internal noise, doubling the prediction horizon. Furthermore, we demonstrate on chaotic dynamical systems that this design enables robust estimation of the full Lyapunov spectrum (100% success rate across 50 seeds), signifying that the autonomous RC faithfully emulates the essential properties of the target dynamical system. This work provides a systematic explanation for a common RC failure mode and offers a concrete design guideline, advancing RCs from heuristic trial-and-error tuning toward a reliable tool for modeling complex systems.

1 Main

Chaotic phenomena [1, 2], governed by deterministic laws yet exhibiting sensitive dependence on initial conditions (“butterfly effect”) and aperiodic behavior, are ubiquitous across fields ranging from meteorology to neuroscience. The long-term behavior

of such systems settles onto a bounded invariant set—an attractor. Even in low-dimensional systems, these attractors often possess complex fractal geometries, making the prediction and modeling of the underlying dynamics fundamentally challenging. Applying machine learning to chaotic time-series analysis encounters hurdles inherent to this complex nature. Conventional data-driven approaches, including standard recurrent neural networks (RNNs), often struggle not only with technical issues like exploding gradients [3] but also with the fundamental difficulty of learning the global geometric structure of the attractor from finite observations, thereby failing to capture the system’s long-term ergodic properties [4, 5].

To address these challenges, Reservoir Computing (RC) [6, 7] has emerged as a compelling paradigm. Unlike fully trainable networks, RC employs a fixed, randomly generated internal network (the reservoir) to project inputs into a high-dimensional state space, requiring training only for the readout layer via linear regression (Fig. 1a,b). This simplified training approach circumvents the exploding/vanishing gradient problems and achieve remarkable success in modeling chaotic time series [8, 9]. This success is attributed to the preservation of the original dynamical system’s geometrical structure (attractor reconstruction [10, 11]) within the reservoir state space [12, 13], enabling the reproduction of not only short-term predictions but also the system’s crucial invariant properties, such as Lyapunov exponents, attractor dimension, and bifurcation [8, 14, 15].

However, the topological/geometrical reconstruction of the attractor alone does not guarantee the faithful reproduction of the dynamical system, especially during closed-loop (autonomous) operation (Fig. 1a,b). A critical problem arises when the reconstruction is transversally unstable within the reservoir space: trajectories diverge from the attractor, leading to behavior entirely different from the original dynamical system (Fig. 1i). This suggests that closed-loop RC may be an unreliable model that fails to reflect the physical properties of the target dynamical system and only coincidentally succeeds in short-term prediction. Stabilization of the reconstructed attractor is key to this problem, but a systematic method to guarantee this at the design stage has not yet been established. Conventional studies have been limited to achieving stability indirectly through *a posteriori* hyperparameter tuning based on performance metrics like prediction accuracy or errors in the dynamical system’s invariants [16].

Here, we propose a design principle for RC that offers an *a priori* solution to stabilize this reconstruction. From preliminary experiments, we observed that such divergence during closed-loop execution is caused by the spillover [17, 18] of closed-loop eigenmodes: modes that should remain stable migrate into neutral or unstable regions, leading to spurious dynamics (Fig. 1g,h). To address this, we developed an RC design method (Fig. 1d) that explicitly constrains the acquired degrees of freedom, inspired by linear control theory [17–21]. Our central idea is to restrict the subspace where the attractor is embedded to a low-dimensional and globally attractive manifold within the reservoir state space prior to learning. This constraint ensures the stability of the reconstruction by suppressing the excitation of modes outside this subspace (Fig. 1e,f).

We demonstrate, through extensive numerical experiments using diverse chaotic dynamical systems, that this new design principle and its implementation not only dramatically improve the stability of attractor reconstruction but also achieve stable

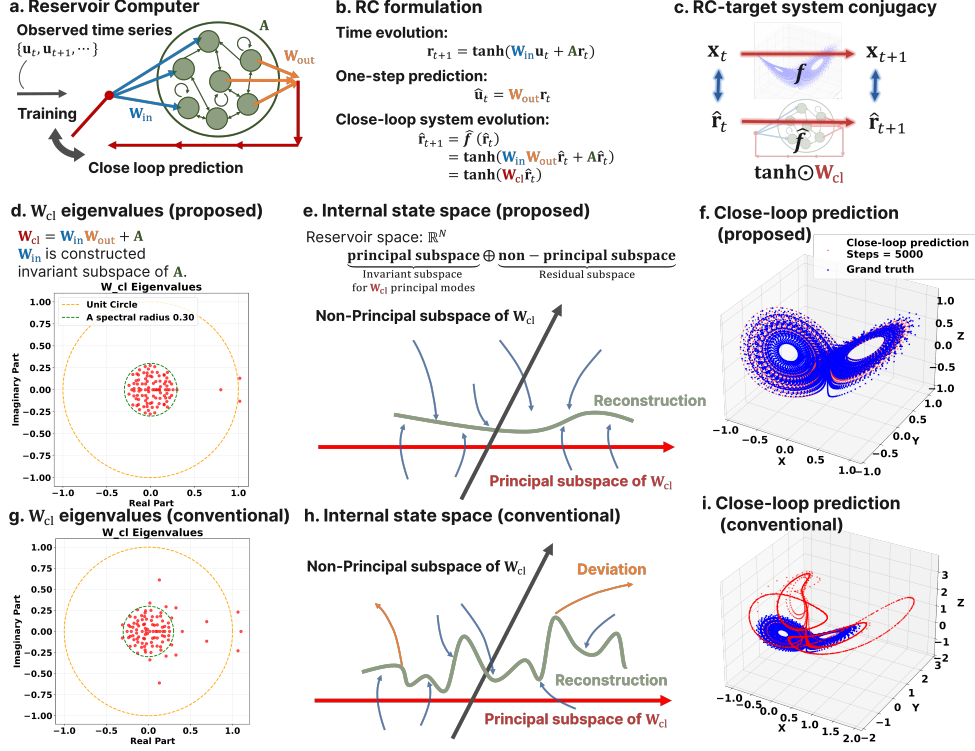


Fig. 1 **a**, Schematic of the Reservoir Computing (RC) framework. During the training phase (switch left, open-loop), the RC is driven by the observed time series \mathbf{u}_t . For autonomous prediction (switch down, closed-loop), the RC uses its own one-step-ahead prediction $\hat{\mathbf{u}}_t$ as the input for the next time step $t + 1$. **b**, General formulation of the discrete-time RC dynamics employed in this study. **c**, Conceptual diagram of topological (semi-)conjugacy. An ideally designed closed-loop RC dynamics \hat{f} becomes topologically (semi-)conjugate to the target dynamical system f , enabling faithful emulation of the original dynamics. **d–f**, Performance of the proposed deterministic input layer design. **d**, Eigenvalue spectrum of the closed-loop matrix \mathbf{W}_{cl} . By design, only the three eigenvalues corresponding to the learnable modes exhibit large magnitudes, while the remaining non-principal eigenvalues are strictly confined within the stable region defined by the spectral radius of \mathbf{A} (green circle), suppressing spurious modes. **e**, Schematic of the reservoir state space. The reconstruction of the target system’s invariant set is confined to a low-dimensional attractive manifold within the reservoir space, ensuring transversal stability. **f**, Long-term autonomous prediction trajectory, accurately and stably reproducing the Lorenz attractor. **g–i**, Instability in the conventional (random) input layer design. **g**, Eigenvalue spectrum of \mathbf{W}_{cl} , showing the uncontrolled eigenvalue spectrum and the emergence of spurious modes, where some eigenvalues spill over the spectral radius of \mathbf{A} (green circle). **h**, Instability induced by spurious modes causes trajectories to diverge from the reconstruction. **i**, Long-term autonomous prediction trajectory, which diverges from the true attractor and exhibits spurious behavior unfaithful to the target dynamics.

long-term prediction that is robust against the randomness inherent in reservoir construction. Furthermore, it enables the accurate estimation of the system’s dynamical invariants, including the full Lyapunov spectrum (specifically the negative exponents) and attractor dimension, which has long been a challenging problem [22, 23]. These

results indicate that the closed-loop RC constructed by our proposed method faithfully mimics the properties of the target dynamical system, suggesting the potential for realizing essentially equivalent modeling (topological semi-conjugacy) (Fig. 1c). In this sense, this work positions RC as a reliable tool for data-driven chaos modeling (e.g., in meteorology and neuroscience).

2 Results

2.1 Suppression of Redundant Unstable-Neutral Modes Stabilizes Attractor Reconstruction

The closed-loop dynamics of a learned RC can be described as the following autonomous dynamical system with respect to the reservoir state \mathbf{r}_t (see Methods for the standard RC framework):

$$\mathbf{r}_{t+1} = \tau(\mathbf{A}\mathbf{r}_t + \mathbf{W}_{\text{in}}\mathbf{W}_{\text{out}}\mathbf{r}_t + \mathbf{b}) = \tau(\mathbf{W}_{\text{cl}}\mathbf{r}_t + \mathbf{b}),$$

where we consider an RC with N nodes and D input dimensions, parameterized by a reservoir transition matrix $\mathbf{A} \in \mathbb{R}^{N \times N}$, an input weight matrix $\mathbf{W}_{\text{in}} \in \mathbb{R}^{N \times D}$, a bias vector $\mathbf{b} \in \mathbb{R}^N$, and the element-wise activation function τ (specifically, we set $\tau(x) = \tanh(x)$). The readout weight matrix $\mathbf{W}_{\text{out}} \in \mathbb{R}^{D \times N}$ is obtained through linear regression. We define $\mathbf{W}_{\text{cl}} := \mathbf{A} + \mathbf{W}_{\text{in}}\mathbf{W}_{\text{out}}$ as the closed-loop matrix. The properties of \mathbf{W}_{cl} are considered to play a crucial role in the closed-loop behavior; for instance, in the case of a linear activation function, the closed-loop RC is equivalent to a linear discrete-time dynamical system, where the dynamics are governed entirely by the eigenvalues of \mathbf{W}_{cl} .

In this section, we first numerically demonstrate that in standard RC (where \mathbf{A} and \mathbf{W}_{in} are randomly generated), the uncontrolled proliferation of unstable or neutral eigenvalues in the closed-loop matrix \mathbf{W}_{cl} causes instability in attractor reconstruction.

In standard RC configurations, no constraints are imposed on the eigenvalue distribution of the post-learning closed-loop matrix \mathbf{W}_{cl} . Consequently, when trained on the Rössler system [24] ($D = 3$) using a standard RC ($N = 200$), multiple eigenvalues are distributed outside the spectral radius of the original \mathbf{A} (green dashed line, Figs. 2a,b). The resulting spectra exhibit cases with explicitly unstable eigenvalues (magnitude > 1 , Fig. 2b) as well as cases with multiple neutral modes (magnitude ≈ 1), even in the absence of strictly unstable modes (Fig. 2b).

To suppress such uncontrolled spectral properties of \mathbf{W}_{cl} , we developed a design principle that deterministically constructs input weight matrix \mathbf{W}_{in} based on the invariant subspace of \mathbf{A} (see Methods for details). Crucially, this principle strictly confine the spectral modifications to a subspace of dimension D a priori. As a result, as shown in Fig. 2c, the number of eigenvalues deviating from the spectrum of \mathbf{A} is exactly $D = 3$, matching theoretical predictions, while the remaining $N - D$ eigenvalues are perfectly preserved from the original reservoir \mathbf{A} .

Next, we demonstrate that the eigenvalue distribution of \mathbf{W}_{cl} has a decisive impact on the stability of attractor reconstruction. Figures 2d–f show the closed-loop prediction trajectories for the RCs corresponding to Figs. 2a–c, respectively. In the standard RC with an unstable mode (Fig. 2a), the trajectory deviates from the original attractor, exhibiting an anomalous convergence to a fixed point (Fig. 2d). In contrast, in cases without explicitly unstable eigenvalues, such as Figs. 2b,c, the systems appear to successfully reproduce the chaotic behavior (Figs. 2e,f). However, as we verify next, this apparent reconstruction is extremely vulnerable to noise perturbations.

To quantitatively evaluate this reconstruction stability, we introduce Basin Stability [25] (S_B) as a metric for robustness against perturbations to the reservoir state. The procedure involves randomly selecting states from the 2000 steps of reservoir states $\{\mathbf{r}_t\}$ driven by the teacher data, applying small uniform noise (drawn from $[-0.001, 0.001]^N$) to define prediction start points, and performing closed-loop prediction. After a transient period of 2000 steps, we verify whether the subsequent 1000 steps of the closed-loop prediction $\{\hat{\mathbf{u}}_t\}$ remain sufficiently close to the true attractor $\{\mathbf{u}_t\}$. Specifically, we check if the directed Hausdorff distance from the prediction to the attractor satisfies $\max_t \min_{t'} \|\hat{\mathbf{u}}_t - \mathbf{u}_{t'}\| < 0.25$. In this study, we generated $N_{\text{test}} = 500$ noise-injected initial points, defining the basin stability as $S_B = M/N_{\text{test}}$, where M denotes the number of trajectories that asymptotically converge to the true attractor. Figures 2g–h visualize the initial points $\hat{\mathbf{u}}_{t_0} = \mathbf{W}_{\text{out}}\mathbf{r}_{t_0}$ mapped to the phase space; points failing to converge are shown as red dots, while those converging are marked with green crosses. In the standard RC (Figs. 2g,h), non-converging points dominate. In contrast, the proposed method (Fig. 2i) achieves a dramatic improvement, with 55% ($= 276/500$) of the points converging to the original attractor.

Figure 2j compares the S_B for standard RC (orange) and the proposed method (green) across varying spectral radii of the reservoir transition matrix \mathbf{A} , evaluated over 10 random seeds. The proposed method achieves significantly higher S_B than the standard method over a wide range of spectral radii of \mathbf{A} . This indicates that *a priori* suppression of the excessive emergence of unstable or neutral eigenvalues in \mathbf{W}_{cl} is essential for ensuring robust stability against noise. Furthermore, the proposed method exhibits a trend of increasing S_B as the spectral radius of \mathbf{A} decreases. This suggests that confining the $N - D$ unmoved eigenvalues of \mathbf{W}_{cl} in a more stable region contributes to suppressing deviations transversal to the reconstructed attractor.

2.2 Improve reproduction of chaotic dynamics based on Unstable Mode Restriction

Next, we compared the closed-loop prediction performance of RCs constructed using the conventional method versus the proposed method for the Lorenz-63 system [1] ($D = 3$) across 50 different initialization seeds (Fig. 3a). As an evaluation metric, we used the Valid Prediction Time [26] (VPT; time until $\text{NRMSE} < 0.5$) normalized by the maximal Lyapunov exponent λ_{max} (Lyapunov time). The conventional method showed substantial variability and sensitivity to initialization, with a modest average VPT of $8.68 \lambda_{\text{max}}^{-1}$ and several trials completely failing to predict the dynamics. In stark contrast, the proposed method achieved consistent high performance (VPTs:

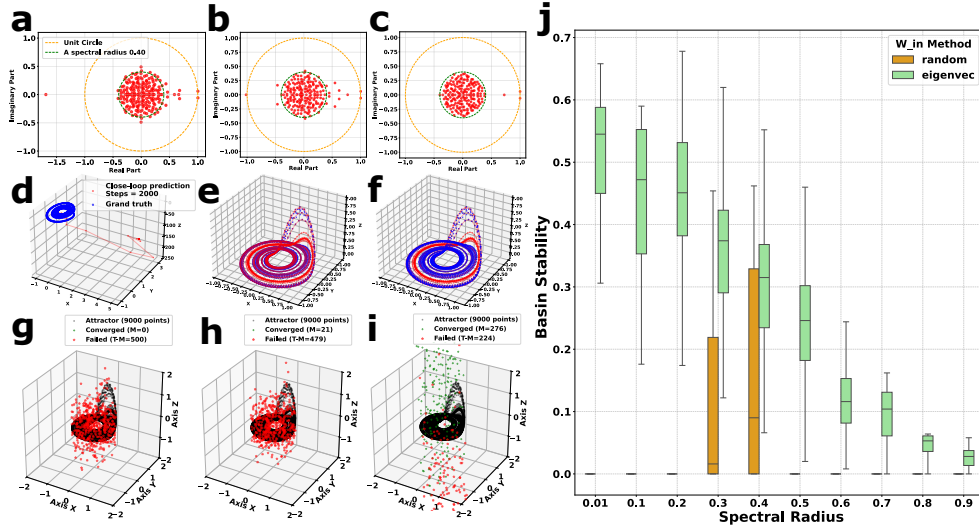


Fig. 2 a–c, Eigenvalue distributions of the closed-loop matrix \mathbf{W}_{cl} . a, b, Conventional random designs (using different random seeds) exhibit eigenvalues that spill over the spectral radius of \mathbf{A} (green dashed circle). c, The proposed deterministic design restricts the spectrum such that only the $D = 3$ eigenvalues corresponding to the learnable modes lie outside the circle, with all remaining modes strictly confined within. d–f, Closed-loop prediction trajectories (red) for the Rössler system plotted against the ground truth (blue), using the RCs corresponding to a, b, and c, respectively. g–i, Basin stability analysis corresponding to d–f. The plots show the initial points ($\hat{\mathbf{u}}_{t_0} = \mathbf{W}_{out}\mathbf{r}_{t_0}$, derived from perturbed reservoir states) which subsequently deviated from the original attractor (red) versus those that successfully converged (green). Note that the conventional model in h appears stable in trajectory (e) but is actually fragile to perturbations. j, Dependence of Basin Stability (S_B) on the spectral radius ρ of \mathbf{A} . The proposed method (green) consistently outperforms the conventional method (orange). Error bars represent the standard deviation over 10 random seeds.

12.06–20.32); its average nearly doubled to 16.05, and remarkably, its worst-case performance (12.06) exceeded the conventional method’s average. This demonstrates the proposed method’s robustness against random reservoir construction. Notably, this performance surpasses reported values for standard RCs [8, 9, 27, 28] and is competitive with optimized RCs [29].

Furthermore, to assess the fidelity of the reproduced long-term statistical properties (often referred to as the system’s “climate” [8, 9]), we estimated the Lyapunov spectrum (LS) from the trained RCs and compared the results with the true values (Figs. 3b,c). For the conventional method (Fig. 3c), the estimated LS ($\hat{\lambda}_1, \hat{\lambda}_2, \hat{\lambda}_3$) deviated significantly from the true values (for Lorenz: $\lambda_1, \lambda_2, \lambda_3 = 0.91, 0, -14.57$) in 36 out of 50 seeds. Crucially, the frequent emergence of multiple spurious positive exponents indicates the existence of positive transverse Lyapunov exponents. Transverse Lyapunov exponents [9, 30] represent the Lyapunov spectrum associated with the response system, excluding the intrinsic exponents of the driving system. Here, a positive transverse exponent signifies transversal instability in the reconstruction. This generation of spurious unstable exponents due to high-dimensional reconstruction is a known consequence of overembedding [22, 31, 32].

In contrast, the proposed method (Fig. 3b) successfully estimated all three Lyapunov exponents, including the negative exponent λ_3 , consistently near the true values across all seeds. This success stems from the reconstruction being effectively restricted to the intended low-dimensional attracting manifold (see Corollary 2). Specifically, this restriction is dynamically enforced by the remaining $N - D$ strongly stable (fast) eigenvalues of \mathbf{W}_{cl} , which cause the state trajectories to rapidly decay onto the manifold associated with the designed D slow modes. Significantly, our method successfully retrieves the negative Lyapunov exponents, a task traditionally considered challenging in attractor reconstruction [22]. This capability enables the reliable estimation of the Kaplan-Yorke dimension [33], which approximates the attractor’s fractal dimension.

In addition to the Lorenz system results, similar results were obtained for the Rössler system (Fig. 3d–f). These results strongly support the central claim of this study: the proposed input layer design effectively controls the spectral properties of the closed-loop RC, thereby substantially improving both the robustness and accuracy of short-term prediction and the fidelity of long-term dynamical system reproduction.

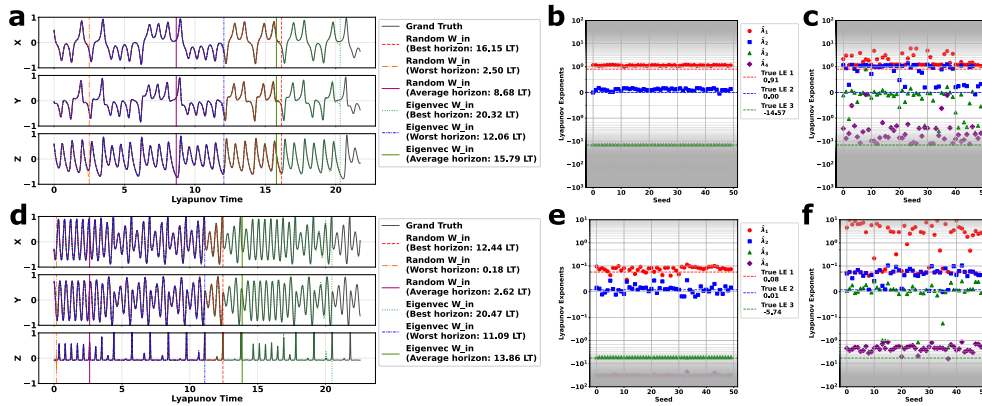


Fig. 3 a–c, Performance evaluation on the Lorenz system. **a**, Comparison of closed-loop prediction trajectories across 50 random initialization seeds. The plots display the best (longest VPT; red/green dashed lines), worst (shortest VPT; orange/blue dashed lines), and average performance (purple/limegreen solid lines) for the conventional and proposed methods, respectively. **b, c**, Estimated Lyapunov spectra $\hat{\lambda}_1, \hat{\lambda}_2, \hat{\lambda}_3, \hat{\lambda}_4$ compared to the true values (dashed line). The y-axis uses a symmetric log scale (linear within $[-1, 1]$). **b**, The proposed method successfully estimates the full spectrum across all 50 seeds. **c**, The conventional method failed in 36 out of 50 seeds, frequently exhibiting spurious positive exponents. **d–f**, Corresponding analysis for the Rössler system. **d**, VPT comparison demonstrating the superior robustness of the proposed method (green/blue/limegreen) over the conventional method (red/orange/purple). **e, f**, Lyapunov spectrum estimation (linear range $[-0.1, 0.1]$). The proposed method (**e**) accurately captures the true spectrum across all seeds, whereas the conventional method (**f**) fails in the majority of trials.

2.3 Parameter Dependency and Design Guidelines

While the proposed method dramatically improves the stability and performance of dynamical system reproduction, its effectiveness may depend on the construction of

the input layer \mathbf{W}_{in} —specifically, on the selection of the D -dimensional invariant subspace associated with the eigenvalues of the reservoir matrix \mathbf{A} .

In this section, we evaluate the impact of invariant subspace selection on performance using the Lorenz-63 system. We sorted the eigenvalues of a 100-dimensional reservoir matrix \mathbf{A} by their real parts and compared the prediction performance (VPT) when constructing \mathbf{W}_{in} from the corresponding invariant subspaces (Figs. 4a–c). For comparison, the performance of the conventional random \mathbf{W}_{in} is also displayed.

Our results demonstrate that regardless of the construction method for \mathbf{A} (random matrix (Fig. 4a), Erdős–Rényi random graph (Fig. 4b), or symmetric matrix (Fig. 4c)), the proposed construction consistently achieves average VPT comparable to or superior to the conventional construction. Notably, across all \mathbf{A} construction methods, setting the spectral radius $\rho = 0.1$ (red bars in Figs. 4a–c) resulted in higher average prediction performance than setting $\rho = 0.3, 0.6$ (blue and green bars). This validates our design philosophy: reducing the spectral radius ρ of \mathbf{A} strengthens the attraction to the reconstruction, thereby effectively restricting divergence from the reconstruction.

We next examine the influence of the reservoir network structure. When \mathbf{A} was constructed as an asymmetric matrix, such as a random matrix or Erdős–Rényi graph (Figs. 4a,b), no clear dependency of performance on the index of the eigenvalues used for \mathbf{W}_{in} was confirmed. In contrast, when a symmetric matrix was used (Fig. 4c), a slight tendency for performance improvement was observed when selecting lower (more negative) eigenvalues for \mathbf{W}_{in} . A complete clarification of this phenomenon is beyond the scope of this study but remains an interesting topic for future research.

Subsequently, we assessed the sensitivity to the spectral radius ρ and regularization parameter β (Fig. 4d). The heatmaps reveal a consistent trend across all reservoir topologies and \mathbf{W}_{in} strategies: superior performance concentrates in the region where both ρ and β are small. This preference for small ρ aligns with our design principle of suppressing dynamics outside the principal subspace, while the effectiveness of small β matches previous reports [29] on the Lorenz-63 system (though this may be system-dependent; see Supplementary Figs. S1–4). Regarding the eigenvalue selection, while asymmetric matrices showed no clear dependency, symmetric matrices exhibited a notable trend where selecting eigenvalues with smaller real parts mitigated performance degradation at larger ρ , consistent with Fig. 4c.

Synthesizing these findings, we propose the following practical design guidelines for RC. First, employ a symmetric matrix (undirected graph) for the reservoir \mathbf{A} . Second, deterministically construct the input weights \mathbf{W}_{in} using the invariant subspace corresponding to the lower (most negative) eigenvalues of \mathbf{A} . This approach eliminates the randomness inherent in \mathbf{W}_{in} and frees us from tuning the hyperparameters associated with it, such as input scaling and input partiality. Consequently, the primary hyperparameters requiring optimization are effectively reduced, allowing us to focus on minimal hyperparameter adjustments.

2.4 Performance across 135 chaotic dynamical systems

To substantiate the universality of the proposed method beyond specific instances like Lorenz and Rössler, we extended our evaluation to a comprehensive benchmark

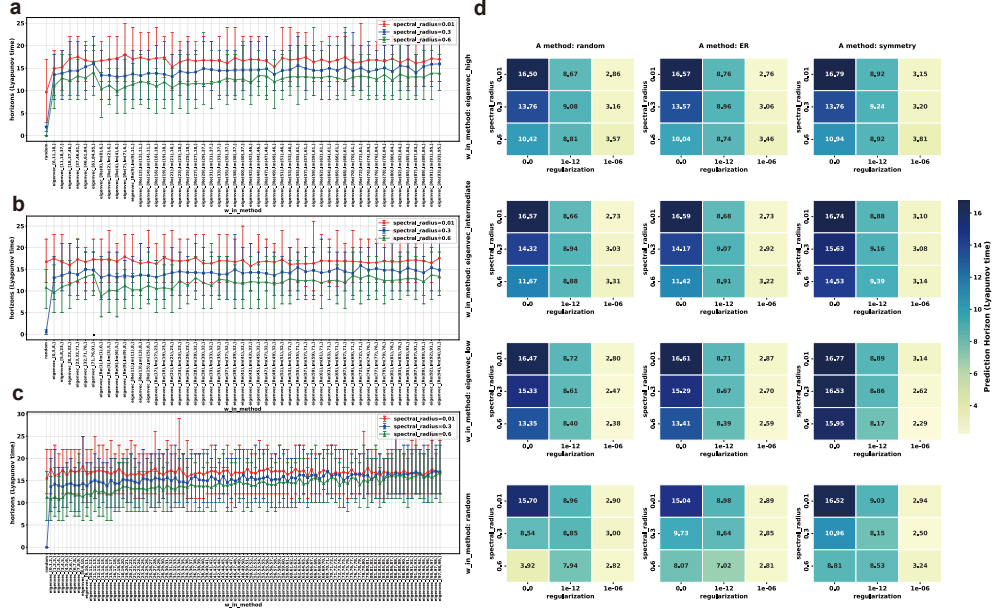


Fig. 4 **a-c**, Dependence of Valid Prediction Time (VPT) on the invariant subspace selection strategy. The x-axis corresponds to the indices of eigenvalues (and associated eigenvectors) used to construct \mathbf{W}_{in} , sorted in ascending order of their real parts. For instance, the label `eigenvec_[1, Re(2), Im(2)]` denotes that \mathbf{W}_{in} was constructed using the eigenvector for the 1st real eigenvalue and the real/imaginary parts of the eigenvector pair for the 2nd complex conjugate eigenvalue. The ‘random’ bar represents the conventional approach. Results are shown for different reservoir topologies: **a**, random matrix; **b**, Erdős–Rényi random graph; and **c**, symmetric matrix. Error bars indicate the standard deviation across 10 random initialization seeds (averages are calculated over 100 prediction start points). **d**, Comprehensive parameter sensitivity analysis. Heatmaps display the average VPT as a function of the spectral radius ρ (y-axis) and regularization parameter β (x-axis). The grid layout is organized by reservoir topology (columns) and \mathbf{W}_{in} construction strategy (rows). Strategies include **random** and the proposed methods selecting eigenvectors with maximal (**high**), median (**intermediate**), and minimal (**low**) real parts.

dataset comprising 135 diverse low-dimensional chaotic dynamical systems from the `dysts` library [34, 35].

As evaluation metrics, we employed VPT (defined earlier) and the SMAPE prediction horizon, the primary metric of the `dysts` benchmark [35]. This metric measures the duration, normalized by the maximal Lyapunov exponent λ_{max} , until the cumulative error ϵ_t exceeds a threshold of 50%, where ϵ_t is defined as
$$\epsilon_t \equiv \frac{200}{t} \sum_{t'=1}^t \frac{\|\mathbf{u}_{t'} - \hat{\mathbf{u}}_{t'}\|}{\|\mathbf{u}_{t'}\| + \|\hat{\mathbf{u}}_{t'}\|}.$$

As a competitive baseline, we referenced the average performance of the top-performing machine learning models (NBEATS [36] / NHiTS [37]) among the 24 forecasting models reported in the comprehensive benchmark by Gilpin [35] (overall average across 135 systems: $13.9 \pm 2.8\lambda_{max}^{-1}$). To align with Gilpin’s experimental conditions we set the reservoir size to $N = 500$ and held other hyperparameters constant, including ρ , β , and the symmetric topology of \mathbf{A} (see Table 2 for details). A

key distinction, however, lies in the time-scale parameter optimization: while Gilpin individually optimized the time-scale parameter (specifically, the leaking rate [38] in the RC context) for each dynamical system, our approach applies a single configuration to all 135 systems without any target-specific optimization. Additionally, as a difference in the evaluation protocol, we constructed RCs using 10 different random seeds and reported the averaged performance metrics to assess the robustness against initialization randomness.

Although these differences in experimental setup must be considered, the RC constructed with the proposed method ($\beta = 0$) achieved an average SMAPE prediction time of $13.3\lambda_{max}^{-1}$ across all 135 systems (Table 1). This is a significant improvement compared to the conventional random-construction RC (average $6.36\lambda_{max}^{-1}$) and is comparable to the results of the (optimized) state-of-the-art deep learning models reported by Gilpin. With slight regularization ($\beta = 1.0 \times 10^{-12}$), similarly high average performance (average $8.75\lambda_{max}^{-1}$) was observed.

Further analysis (Supplementary Figs. S1–S2) reveals heterogeneous performance: while 39 systems showed exceptional long-term accuracy (SMAPE prediction time $> 20\lambda_{max}^{-1}$), 49 systems failed to predict ($< 1\lambda_{max}^{-1}$). Interestingly, however, systems that were difficult to predict under one setting often showed improved performance with just a slight change in the regularization term β (Supplementary Fig. S2).

These results imply that the proposed method, when constrained to fixed parameters, exhibits a form of over-specialization, which can be interpreted as a trade-off stemming from its high capability to faithfully mimic detailed dynamical structures. To enhance generalization across a broader range of dynamical behaviors, a strategy of adaptively adjusting reservoir hyperparameters (particularly β and ρ) according to the target system’s characteristics would be effective. Developing a framework to automatically calibrate these hyperparameters based on target system properties and invariants (e.g., Lyapunov exponents or dimensions), building upon the robust baseline established in this study, represents a crucial direction for future research.

Table 1 Comparison of prediction performance across 135 chaotic systems. The values represent the average SMAPE prediction horizon and Valid Prediction Time (VPT), normalized by Lyapunov times (λ_{max}^{-1}).

Metric	Reference [35]	Proposed RC		Conventional RC	
	NBEATS [36] / NHITS [37]	No Reg. ($\beta = 0$)	Reg. ($\beta = 10^{-12}$)	No Reg. ($\beta = 0$)	Reg. ($\beta = 10^{-12}$)
SMAPE	13.9	13.3	8.75	6.36	5.53
VPT	–	8.99	5.50	4.35	3.42

3 Discussion

This study establishes a deterministic simple design principle for the input layer \mathbf{W}_{in} , offering a direct solution to the long-standing challenge of transversal instability in

the reproduction and prediction of dynamical systems via Reservoir Computing (RC). While previous works demonstrated RC’s capacity to topologically reconstruct attractors [8, 9, 12, 13], no *a priori* method existed to guarantee that its dynamics would not diverge from the attractor, ensuring predictions that faithfully reflect the intrinsic properties of the target dynamical system. We identified that such reconstruction instability stems from the excitation of spurious modes in the closed-loop RC, and successfully suppressed this phenomenon through an *a priori* design of the input layer. By confining the attractor reconstruction to an attractive low-dimensional manifold, the method suppresses deviations from the reconstructed attractor as well as the generation of spurious Lyapunov exponents associated with overembedding [22, 31, 32]. Consequently, our method paves the way for reliable modeling of complex chaotic phenomena and frees RC users from tuning the input layer \mathbf{W}_{in} . It facilitates the accurate estimation of dynamical invariants from complex time series (e.g., neural signals, fluid turbulence), ensuring stable long-term predictions faithful to the underlying physical laws.

Furthermore, owing to its architectural simplicity and ease of learning, RC is increasingly implemented as “physical RC” utilizing diverse physical substrates, such as quantum circuits, photonic systems, and spintronic devices [39]. The deterministic \mathbf{W}_{in} design proposed in this study can serve as a foundational technology to ensure stable operation robust against noise inherent to physical systems, thereby reducing the need for heuristic trial-and-error. Although the internal reservoir transition matrix \mathbf{A} is often unknown or difficult to model explicitly in such physical implementations, our design principle requires only an invariant subspace or a subset of eigenvectors, rather than full knowledge of \mathbf{A} . Established data-driven techniques, such as Subspace Identification Methods (SIM) [40–43] and Dynamic Mode Decomposition (DMD) [44, 45], can effectively estimate the invariant subspace directly from observed time series data. Integrating these data-driven methods with our input layer design framework offers a promising pathway to enhance the reliability of physical RC, establishing it as a robust computational paradigm.

The results of our numerical experiments, particularly under “full observation” conditions, invite a reconsideration of the role of “memory” in RNNs for dynamical system reproduction tasks. In the rigorous embedding theory of RC established by Hart, Grigoryeva et al. [12, 46], which extends Takens’ theorem to reservoir computing, the full-rank condition of the controllability matrix $\mathcal{C} = [\mathbf{W}_{\text{in}}, \mathbf{A}\mathbf{W}_{\text{in}}, \dots, \mathbf{A}^{N-1}\mathbf{W}_{\text{in}}]$ serves as a sufficient condition for a linear RC to encode past information and reconstruct the attractor. Crucially, however, our proposed method constructs \mathbf{W}_{in} from only a few eigenvectors of \mathbf{A} , rendering the controllability matrix rank-deficient and thus explicitly violating this theoretical condition. Furthermore, while a larger spectral radius ρ is typically associated with extended memory retention, our experiments reveal that prediction accuracy maximizes at a very small spectral radius. It might appear from these findings that the explicit RC’s memory is not necessarily required.

This apparent dichotomy is reconciled by distinguishing the observation regimes. The theory of Hart, Grigoryeva et al. addresses the general scenario of partial observation, where the state of the dynamical system is only partially accessible. In such

cases, since the full state cannot be uniquely determined from instantaneous observation alone, it is essential to retain past information as memory to reconstruct the state, analogous to delay-coordinate embedding [10, 11]. In contrast, this study targets the full observation regime, where all state variables are observable. Under this condition, the instantaneous observation contains all necessary information to determine future evolution. This fact supports the design philosophy that, under full observation, confining the reconstruction to the stable manifold takes precedence over maximizing memory capacity. In this sense, our results do not contradict the theory of Hart and Grigoryeva.

Finally, we emphasize that the central design philosophy validated through our numerical experiments—selectively learning only the minimal set of modes essential for reproducing the target dynamics, while rigorously preventing the remaining modes from spilling over from stable regions—is not limited to the specific framework of Reservoir Computing. Rather, it offers a universal perspective applicable to various other state-space models and machine learning methods (e.g. FORCE[47], extreme learning machine[48]). We propose that designing the model architecture to ensure that the reconstruction of the target phenomenon (e.g., attractors or invariant manifolds) embedded within the internal state remains attractive is key to realizing robust and reliable machine learning models.

4 Methods

This section describes the formulation of the Reservoir Computing (RC) model used in this study, the details of the proposed input layer construction method, and the specific settings for the numerical experiments.

4.1 Reservoir Computing Fundamentals and Closed-Loop Operation

We outline the procedure for performing time-series prediction tasks using a standard discrete-time RC model [6, 7, 49, 50]. Consider a target dynamical system f evolving on an invariant set I , where the state $\mathbf{x}_t \in I$ is mapped to a D -dimensional observation vector $\mathbf{u}_t = \mathbf{h}(\mathbf{x}_t)$ via an observation map $\mathbf{h} : I \rightarrow \mathbb{R}^D$. The RC receives this input time series \mathbf{u}_t and updates its N -dimensional reservoir state $\mathbf{r}_t \in \mathbb{R}^N$ according to:

$$\mathbf{r}_{t+1} = \tau(\mathbf{A}\mathbf{r}_t + \mathbf{W}_{\text{in}}\mathbf{u}_t + \mathbf{b}),$$

where $\mathbf{A} \in \mathbb{R}^{N \times N}$, $\mathbf{W}_{\text{in}} \in \mathbb{R}^{N \times D}$, and $\mathbf{b} \in \mathbb{R}^N$ denote the reservoir transition matrix, the input weight matrix, and the bias vector, respectively. In this study, we adopted the hyperbolic tangent $\tau(\cdot) = \tanh(\cdot)$, which is standardly used as the activation function in RC. While these internal parameters are randomly initialized and fixed, the output weight matrix \mathbf{W}_{out} is trained to predict the next state \mathbf{u}_{t+1} . Using ridge regression with a regularization parameter β , the optimal weights are given by:

$$\mathbf{W}_{\text{out}} = \mathbf{Y}\mathbf{R}^T(\mathbf{R}\mathbf{R}^T + \beta\mathbf{I})^{-1},$$

where \mathbf{R} and \mathbf{Y} denote the matrices collecting the reservoir states \mathbf{r}_t and the targets \mathbf{u}_{t+1} , respectively, over T_{train} time steps following an initial warmup period T_{warmup} to eliminate the initial state.

After training, the RC performs autonomous time-series generation (closed-loop prediction). This is achieved by feeding back the model’s output $\hat{\mathbf{u}}_t = \mathbf{W}_{\text{out}}\mathbf{r}_t$ as the input for the next time step. The dynamics of the closed-loop system are then described as the following autonomous dynamical system with respect to the reservoir state \mathbf{r}_t :

$$\mathbf{r}_{t+1} = \tau(\mathbf{A}\mathbf{r}_t + \mathbf{W}_{\text{in}}\mathbf{W}_{\text{out}}\mathbf{r}_t + \mathbf{b}) = \tau(\mathbf{W}_{\text{cl}}\mathbf{r}_t + \mathbf{b}) =: \hat{f}(\mathbf{r}_t), \quad (3)$$

where we define $\mathbf{W}_{\text{cl}} := \mathbf{A} + \mathbf{W}_{\text{in}}\mathbf{W}_{\text{out}}$ as the closed-loop matrix.

The theoretical foundation for RC’s success in modeling dynamical systems lies primarily in the Echo State Property (ESP) [6, 49]. ESP signifies that, when driven by a common input signal, the reservoir states asymptotically converge to a unique trajectory, regardless of the initial reservoir state. When ESP is satisfied, (strong) Generalized Synchronization (GS) [51, 52] is achieved—characterized by the existence of a (smooth) synchronization function Φ mapping the driving target state \mathbf{x}_t to the response reservoir state \mathbf{r}_t i.e. $\mathbf{r}_t = \Phi(\mathbf{x}_t)$ as $t \rightarrow \infty$ [9, 12, 13].

Crucially, if Φ is an embedding (a diffeomorphism onto its image), a set topologically equivalent to the target invariant set is reconstructed within the reservoir state space. This geometric reconstruction is conceptually analogous to the delay-coordinate embedding [10, 11], providing the theoretical justification for RC to reproduce dynamical invariants and generate predictions preserving the original system properties [8].

However, the static geometric reconstruction of the invariant set I (where $\Phi(I)$ is the reconstructed attractor) does not theoretically guarantee the successful reproduction of the dynamics. For ideal reproduction, the closed-loop dynamics \hat{f} of the RC must be topologically (semi-)conjugate to the target dynamics f ; that is, the map Φ must satisfy the commutativity condition $\hat{f} \circ \Phi = \Phi \circ f$ on I . Furthermore, for robust physical realizability, the reconstructed attractor $\Phi(I)$ must be an asymptotically stable invariant set under \hat{f} . This implies that $\Phi(I)$ must be attractive in the directions transversal to the reconstruction. This transversal stability (stability of GS) is quantitatively characterized by the Transverse Lyapunov Exponents (TLEs), defined as the set difference between the Lyapunov spectrum of the response system and that of the drive system. A necessary condition for stable GS is that all TLEs are negative [52, 53].

Despite its importance, a systematic method to ensure stable GS *a priori* has not been established. Conventional approaches rely on *a posteriori* hyperparameter optimization based on prediction error or Lyapunov spectra [16]. Consequently, the learned RC often exhibits positive TLEs depending on random initialization, leading to trajectory divergence from $\Phi(I)$ or capture by “untrained attractors” [54–56] (see also Fig.1i). This instability is fundamentally linked to the phenomenon of “overembedding” [22, 31, 32]: embedding the attractor into an unnecessarily high-dimensional state space complicates the geometry of the reconstruction, inducing spurious positive Lyapunov exponents that destabilize the synchronization.

4.2 Deterministic Input Layer Construction (Proposed method)

As discussed in the previous section, standard RC configurations frequently exhibit instability during closed-loop operation, failing to faithfully reproduce the target dynamics. Numerical experiments confirmed that this reconstruction instability stems from the presence of excessive spurious eigenvalues in the closed-loop matrix \mathbf{W}_{cl} (see Results). To address this problem, this study proposes a new simple design principle to directly control the eigenvalue distribution of \mathbf{W}_{cl} , inspired by linear control theory [17–21].

Specifically, we construct the columns of the input matrix $\mathbf{W}_{\text{in}} \in \mathbb{R}^{N \times D}$ from the invariant subspace of the reservoir transition matrix $\mathbf{A} \in \mathbb{R}^{N \times N}$. First, we compute all eigenvectors of \mathbf{A} . Next, we select D linearly independent real basis vectors $\{\mathbf{x}_1, \dots, \mathbf{x}_D\}$ to span the target invariant subspace. For instance, for real eigenvalues, the corresponding real eigenvectors are selected directly; for complex conjugate eigenvalue pairs, the real and imaginary parts of the eigenvectors are used to ensure \mathbf{W}_{in} remains real-valued. These selected vectors are normalized and arranged as columns to form the input matrix \mathbf{W}_{in} :

$$\mathbf{W}_{\text{in}} = \left[\frac{\mathbf{x}_1}{\|\mathbf{x}_1\|}, \frac{\mathbf{x}_2}{\|\mathbf{x}_2\|}, \dots, \frac{\mathbf{x}_D}{\|\mathbf{x}_D\|} \right]. \quad (1)$$

By this construction, the column space of \mathbf{W}_{in} , denoted as $\text{Im}(\mathbf{W}_{\text{in}})$, coincides with the D -dimensional real invariant subspace of \mathbf{A} , defined as $V_D = \text{span}\{\mathbf{x}_1, \dots, \mathbf{x}_D\}$ (i.e., $\text{Im}(\mathbf{W}_{\text{in}}) = V_D$).

Given this construction of \mathbf{W}_{in} , we establish the following theorem regarding the spectral properties of the closed-loop matrix $\mathbf{W}_{\text{cl}} = \mathbf{A} + \mathbf{W}_{\text{in}}\mathbf{W}_{\text{out}}$.

Theorem 1 (Invariant Eigenvalues). *Let $\mathbf{A} \in \mathbb{R}^{N \times N}$ be a real matrix possessing a D -dimensional real invariant subspace V_D . Let the eigenvalues of the restriction $\mathbf{A}|_{V_D}$ be $\{\lambda_1, \dots, \lambda_D\}$, and let the remaining eigenvalues be $\{\lambda_{D+1}, \dots, \lambda_N\}$. If a matrix $\mathbf{B} \in \mathbb{R}^{N \times D}$ satisfies $\text{Im}(\mathbf{B}) \subseteq V_D$ (i.e., the column vectors of \mathbf{B} are contained in V_D), then for any real matrix $\mathbf{C} \in \mathbb{R}^{D \times N}$, the spectrum of $\mathbf{A}' = \mathbf{A} + \mathbf{B}\mathbf{C}$ contains the multiset $\{\lambda_{D+1}, \dots, \lambda_N\}$.*

Proof The proof is provided in Supplementary Information. □

This theorem guarantees that when \mathbf{W}_{in} is constructed from a D -dimensional real invariant subspace V_D of \mathbf{A} as in the proposed method, $N - D$ of the closed-loop matrix \mathbf{W}_{cl} 's eigenvalues remain unchanged from the original matrix \mathbf{A} , regardless of the learned \mathbf{W}_{out} . Therefore, by designing \mathbf{A} in advance such that its eigenvalues have sufficiently small absolute values (e.g., by setting a small spectral radius ρ), the absolute values of the $N - D$ non-principal, invariant eigenvalues can be kept small.

Corollary 2 (Inheritance of Invariant Subspace). *Under the assumptions of Theorem 1, the subspace V_D remains an invariant subspace of the closed-loop matrix $\mathbf{A}' =$*

$\mathbf{A} + \mathbf{BC}$. Consequently, the D eigenvalues of \mathbf{A}' that are not invariant (i.e., modifiable by \mathbf{C}) correspond to the eigenvalues of the restriction $\mathbf{A}'|_{V_D}$.

Proof The proof is provided in Supplementary Information. \square

This theorem can be interpreted through the analogy of a linear RC (where the activation function is the identity map). In the linear case, Corollary 2 implies that the invariant subspace corresponding to the eigenvalues modified by learning (representing the “slow” dynamics of the closed-loop RC) strictly coincides with the column space of \mathbf{W}_{in} . By designing \mathbf{A} with a sufficiently small spectral radius, the remaining $N - D$ modes become fast and stable, ensuring the exponential stability of the trajectory towards this slow subspace.

In actual RC systems, although the effect of the activation function’s nonlinearity must be considered, we consider that a corresponding “slow” invariant submanifold exists in the vicinity of the column space of \mathbf{W}_{in} , where the attractor is embedded. Thanks to the clear separation between the learned slow dynamics and the fast stable dynamics, this submanifold becomes low-dimensional and attractive. Through this mechanism, the reconstructed attractor becomes transversally stable, thereby suppressing the generation of spurious Lyapunov exponents and enabling robust long-term prediction.

4.3 Experimental Setup

For the numerical experiments, we utilized the `dysts` benchmark library [34, 35], which comprises 135 diverse low-dimensional chaotic dynamical systems. Prior to feeding the data into the RC, each state variable was preprocessed via dimension-wise linear scaling to map the values to the range $[-1, 1]$. The detailed analyses presented in the Results section were conducted using the Rössler [24] and Lorenz-63 [1] systems selected from this data setting.

The RC model configuration adheres to the formulation described in Eq. (1). Unless otherwise specified, the common hyperparameters listed in Table 2 were used in the experiments. We evaluated three distinct topologies for the reservoir transition matrix \mathbf{A} : a random matrix (generated from a uniform distribution), an Erdős–Rényi random graph, and a symmetric random matrix (generated from a uniform distribution). In all instances, the matrix was rescaled so that its spectral radius matched the target value ρ . For the input weight matrix \mathbf{W}_{in} , we compared the conventional random initialization (where elements are drawn from a uniform distribution and each column is normalized to unit norm) with our proposed deterministic construction based on the invariant subspace of \mathbf{A} (as detailed in Sec. 4.2). The output weight matrix \mathbf{W}_{out} was optimized via ridge regression. The bias vector \mathbf{b} and initial state \mathbf{r}_0 were generated by sampling from a uniform distribution within the specified range. Crucially, our proposed deterministic method eliminates standard RC hyperparameters, such as input strength scaling and sparsity, simplifying the design process.

As for the evaluation procedure, short-term prediction performance was evaluated by performing closed-loop prediction and calculating the Valid Prediction Time (VPT). VPT is defined as the time duration, normalized by the maximal Lyapunov

Table 2 List of hyperparameters and experimental settings. Values denote the specific settings used for the results presented in the corresponding figures and table.

Parameter	Symbol	Description	Figs. 1,2	Fig. 3	Fig. 4	Table 1
Reservoir size	N	Number of reservoir nodes	200	200	100	500
Spectral radius	ρ	Spectral radius of \mathbf{A}	0.4	0.1	0.01, 0.3, 0.6	0.1
Connection probability	p_A	Edge probability (random graph)	0.3	0.3	0.3	–
Regularization	α	Ridge regression coefficient	0	0	$0, 10^{-6}, 10^{-12}$	$0, 10^{-12}$
Bias distribution	\mathbf{b}	Uniform distribution range	$[-10^{-3}, 10^{-3}]$	$[-10^{-3}, 10^{-3}]$	$[-0.01, 0.01]$	$[-0.01, 0.01]$
Warmup steps	T_{warm}	Steps to wash out reservoir initial transients	1000	1000	1000	100
Training steps	T_{train}	Steps used for optimizing \mathbf{W}_{out}	2000	2000	2000	900
Test trials	N_{test}	Number of prediction start points	500	–	100	100

exponent λ_{\max} , until the Normalized Root Mean Square Error (NRMSE) exceeds a threshold of 0.5:

$$\text{NRMSE}(\hat{\mathbf{u}}_t) = \sqrt{\frac{1}{D} \sum_{i=1}^D \frac{(\hat{u}_{t,i} - u_{t,i})^2}{\sigma_i^2}},$$

$$\text{VPT} = \frac{1}{\lambda_{\max}} \operatorname{argmax}_{t_f} \{t_f \mid \text{NRMSE}(\hat{\mathbf{u}}_t) < 0.5, \forall t \leq t_f\},$$

where D is the dimension of the system and σ_i^2 denotes the variance of the i -th dimension of the target time series. For the large-scale benchmark involving 135 systems, we also employed the cumulative SMAPE metric defined as:

$$\epsilon_t \equiv \frac{200}{t} \sum_{t'=1}^t \frac{\|\mathbf{u}_{t'} - \hat{\mathbf{u}}_{t'}\|}{\|\mathbf{u}_{t'}\| + \|\hat{\mathbf{u}}_{t'}\|}.$$

These evaluations were conducted over N_{test} distinct prediction start points, and the average value was reported as the performance metric.

To assess the fidelity of the attractor reproduction, we estimated the Lyapunov spectrum of the closed-loop RC. The estimation utilized a standard algorithm [57, 58] based on QR decomposition of the product of Jacobians. Specifically, we computed

the Jacobian $D\hat{f}(\mathbf{r}_t)$ of the closed-loop map \hat{f} along the trajectory:

$$D\hat{f}(\mathbf{r}_t) = \frac{d\hat{f}(\mathbf{r}_t)}{d\mathbf{r}_t} = \text{diag}(1 - \tanh^2(\mathbf{W}_{\text{cl}}\mathbf{r}_t + \mathbf{b}))\mathbf{W}_{\text{cl}} = \text{diag}(1 - \mathbf{r}_{t+1}^2)\mathbf{W}_{\text{cl}}.$$

Note that the last term utilizes the updated state from Eq. (1) for efficient computation. For calculation of transverse Lyapunov exponents, the trajectory $\{\mathbf{r}_t\}$ was generated by driving the reservoir with the true input during the training period.

Acknowledgements. This work was supported by JSPS KAKENHI Grant Number JP25KJ1714, JST ALCA-Next Grant No. JPMJAN23F2 and JST Moonshot R&D Grant No. JPMJMS2021, JST PRESTO Grant No. JPMJPR25K5, JST CREST Grant No. JPMJCR25R1.

5 Supplementary information

5.1 Theoretical Foundation

Theorem 1 (Invariant Eigenvalues). *Let $\mathbf{A} \in \mathbb{R}^{N \times N}$ be a real matrix possessing a D -dimensional real invariant subspace V_D . Let the eigenvalues of the restriction $\mathbf{A}|_{V_D}$ be $\{\lambda_1, \dots, \lambda_D\}$, and let the remaining eigenvalues be $\{\lambda_{D+1}, \dots, \lambda_N\}$. If a matrix $\mathbf{B} \in \mathbb{R}^{N \times D}$ satisfies $\text{Im}(\mathbf{B}) \subseteq V_D$ (i.e., the column vectors of \mathbf{B} are contained in V_D), then for any real matrix $\mathbf{C} \in \mathbb{R}^{D \times N}$, the spectrum of $\mathbf{A}' = \mathbf{A} + \mathbf{BC}$ contains the multiset $\{\lambda_{D+1}, \dots, \lambda_N\}$.*

Proof Choose a basis \mathbf{P}_D for the invariant subspace V_D and extend it to form a basis $\mathbf{P} = [\mathbf{P}_D, \mathbf{P}_{N-D}]$ for \mathbb{R}^N . Consider the similarity transformation $\tilde{\mathbf{A}} = \mathbf{P}^{-1}\mathbf{A}\mathbf{P}$. Since V_D is \mathbf{A} -invariant, $\tilde{\mathbf{A}}$ assumes a block upper triangular form:

$$\tilde{\mathbf{A}} = \begin{pmatrix} \mathbf{A}_{11} & \mathbf{A}_{12} \\ \mathbf{0} & \mathbf{A}_{22} \end{pmatrix},$$

where the eigenvalues of \mathbf{A}_{22} correspond to the complementary set $\{\lambda_{D+1}, \dots, \lambda_N\}$.

Next, consider the term \mathbf{BC} . Since $\text{Im}(\mathbf{B}) \subseteq V_D = \text{Im}(\mathbf{P}_D)$, the transformed matrix $\tilde{\mathbf{B}} = \mathbf{P}^{-1}\mathbf{B}$ takes the form:

$$\tilde{\mathbf{B}} = \begin{pmatrix} \mathbf{B}_1 \\ \mathbf{0} \end{pmatrix},$$

where $\mathbf{B}_1 \in \mathbb{R}^{D \times D}$. Let us partition the transformed matrix $\mathbf{C}\mathbf{P}$ as $[\mathbf{C}_1, \mathbf{C}_2]$, where $\mathbf{C}_1 \in \mathbb{R}^{D \times D}$ and $\mathbf{C}_2 \in \mathbb{R}^{D \times (N-D)}$. The similarity transformation of the closed-loop matrix $\mathbf{A}' = \mathbf{A} + \mathbf{BC}$ is then given by:

$$\begin{aligned} \tilde{\mathbf{A}}' &= \mathbf{P}^{-1}(\mathbf{A} + \mathbf{BC})\mathbf{P} \\ &= \tilde{\mathbf{A}} + \tilde{\mathbf{B}}(\mathbf{C}\mathbf{P}) \\ &= \begin{pmatrix} \mathbf{A}_{11} & \mathbf{A}_{12} \\ \mathbf{0} & \mathbf{A}_{22} \end{pmatrix} + \begin{pmatrix} \mathbf{B}_1 \\ \mathbf{0} \end{pmatrix} (\mathbf{C}_1 \ \mathbf{C}_2) \\ &= \begin{pmatrix} \mathbf{A}_{11} & \mathbf{A}_{12} \\ \mathbf{0} & \mathbf{A}_{22} \end{pmatrix} + \begin{pmatrix} \mathbf{B}_1\mathbf{C}_1 & \mathbf{B}_1\mathbf{C}_2 \\ \mathbf{0} & \mathbf{0} \end{pmatrix} \\ &= \begin{pmatrix} \mathbf{A}_{11} + \mathbf{B}_1\mathbf{C}_1 & \mathbf{A}_{12} + \mathbf{B}_1\mathbf{C}_2 \\ \mathbf{0} & \mathbf{A}_{22} \end{pmatrix}. \end{aligned}$$

The spectrum of the block triangular matrix $\tilde{\mathbf{A}}'$ is the union of the spectra of its diagonal blocks. The bottom-right block remains exactly \mathbf{A}_{22} regardless of \mathbf{C} . Thus, the spectrum of \mathbf{A}' always includes the eigenvalues of \mathbf{A}_{22} , which are $\{\lambda_{D+1}, \dots, \lambda_N\}$. \square

Corollary 2 (Inheritance of Invariant Subspace). *Under the assumptions of Theorem 1, the subspace V_D remains an invariant subspace of the closed-loop matrix $\mathbf{A}' = \mathbf{A} + \mathbf{B}\mathbf{C}$. Consequently, the D eigenvalues of \mathbf{A}' that are not invariant (i.e., modifiable by \mathbf{C}) correspond to the eigenvalues of the restriction $\mathbf{A}'|_{V_D}$.*

Proof We show that V_D is invariant under \mathbf{A}' . Let \mathbf{v} be any vector in V_D . We compute $\mathbf{A}'\mathbf{v}$:

$$\mathbf{A}'\mathbf{v} = (\mathbf{A} + \mathbf{B}\mathbf{C})\mathbf{v} = \mathbf{A}\mathbf{v} + \mathbf{B}(\mathbf{C}\mathbf{v}).$$

First, since V_D is \mathbf{A} -invariant, $\mathbf{A}\mathbf{v} \in V_D$. Second, note that $\mathbf{w} := \mathbf{C}\mathbf{v}$ is a vector in \mathbb{R}^D . Since $\text{Im}(\mathbf{B}) \subseteq V_D$, the vector $\mathbf{B}\mathbf{w} = \mathbf{B}(\mathbf{C}\mathbf{v})$ must lie within V_D . Since V_D is a subspace (closed under addition), the sum $\mathbf{A}\mathbf{v} + \mathbf{B}\mathbf{C}\mathbf{v}$ belongs to V_D . Therefore, $\mathbf{A}'\mathbf{v} \in V_D$ for all $\mathbf{v} \in V_D$, proving that V_D is an invariant subspace of \mathbf{A}' . \square

5.2 Benchmark Evaluation Details

To comprehensively evaluate the performance of the proposed method in chaotic time-series forecasting, we conducted comparative experiments adhering to the benchmark protocol established by Gilpin [34, 35]. As detailed in Appendix A of his work [35], this extensive benchmark evaluates 24 distinct forecasting models, ranging from classical statistical methods to state-of-the-art deep learning architectures. However, we introduced two key methodological distinctions. First, to enhance the robustness of the performance evaluation, we reported the average metrics calculated over 10 different random seeds and 100 different prediction start points, providing a more statistical assessment than relying on a single initialization. Second, as emphasized in the main text, we did not optimize the leaking rate for each target dynamical system; instead, we used an RC configured with fixed parameters. This is because we observed that the performance of our proposed configuration was relatively insensitive to variations in the leaking rate.

Regarding the training data size, we adopted the settings from Gilpin’s ESN model: warmup steps $T_{\text{warm}} = 100$ and training steps $T_{\text{train}} = 900$. Recognizing that this constitutes a very limited dataset for chaotic system identification, we additionally performed experiments with an extended data regime ($T_{\text{warm}} = 1000, T_{\text{train}} = 2000$) to assess the model’s potential under more favorable conditions (Fig. S5).

The `dysts` dataset consists of non-delayed autonomous (114 systems), delayed autonomous (15 systems), and non-autonomous (6 systems) equations. When using the proposed method ($\beta = 0$), as shown in Fig. S1, we observed a significant disparity in prediction performance depending on the system classification. Specifically, while the method achieved high performance on some non-delayed autonomous systems, it failed to predict almost all delayed autonomous and non-autonomous systems. This limitation is likely attributed to the standard RC framework adopted in this study, which lacks explicit mechanisms to handle delay terms or external driving forces. However, we found that introducing a slight regularization ($\beta = 1.0 \times 10^{-12}$) resulted

in marginal performance improvements, even for those systems where prediction had initially failed completely.

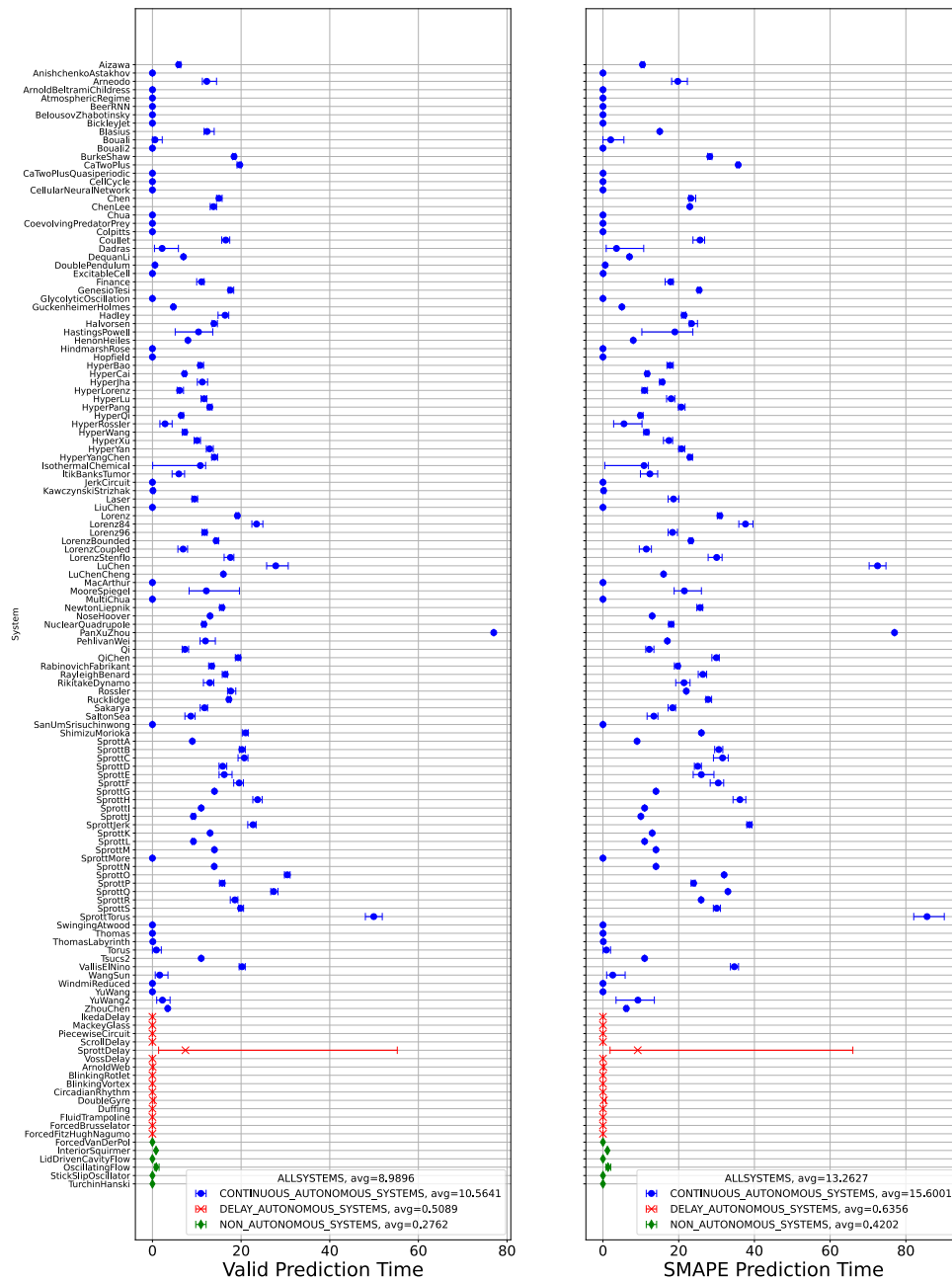


Fig. S2 Results evaluated using the same metrics and format as Fig. S1.

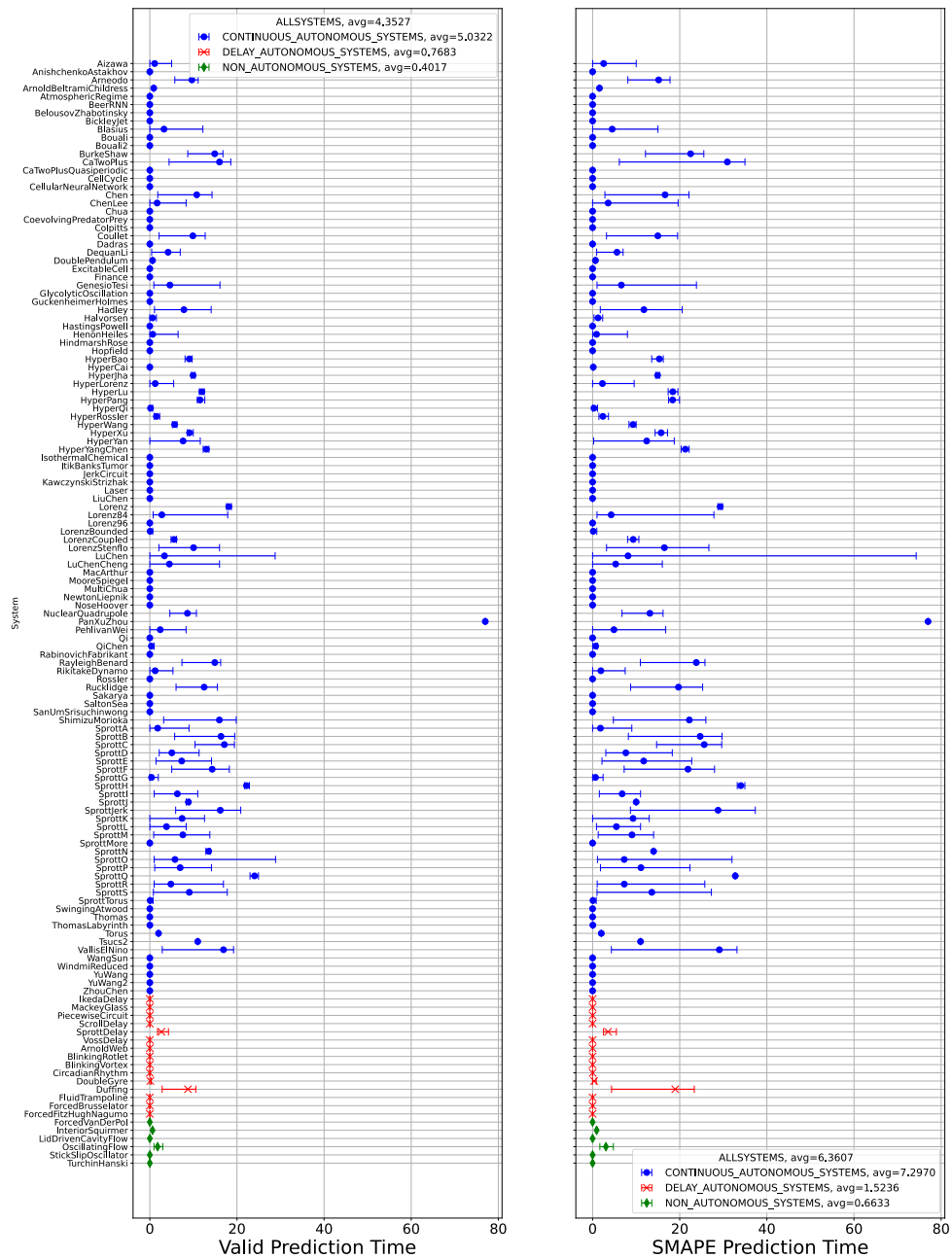


Fig. S3 Results evaluated using the same metrics and format as Fig. S1.

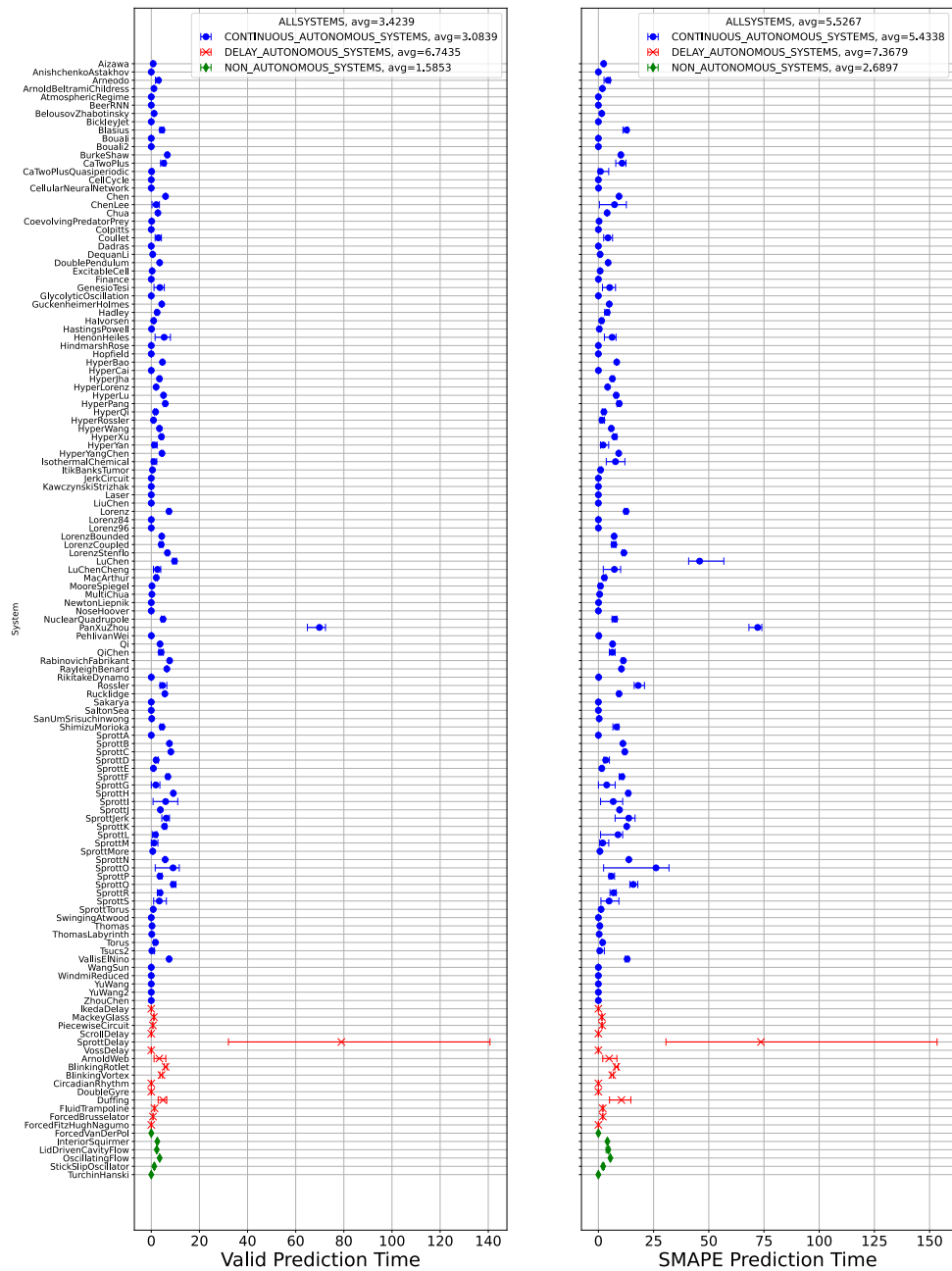


Fig. S4 Results evaluated using the same metrics and format as Fig. S1.

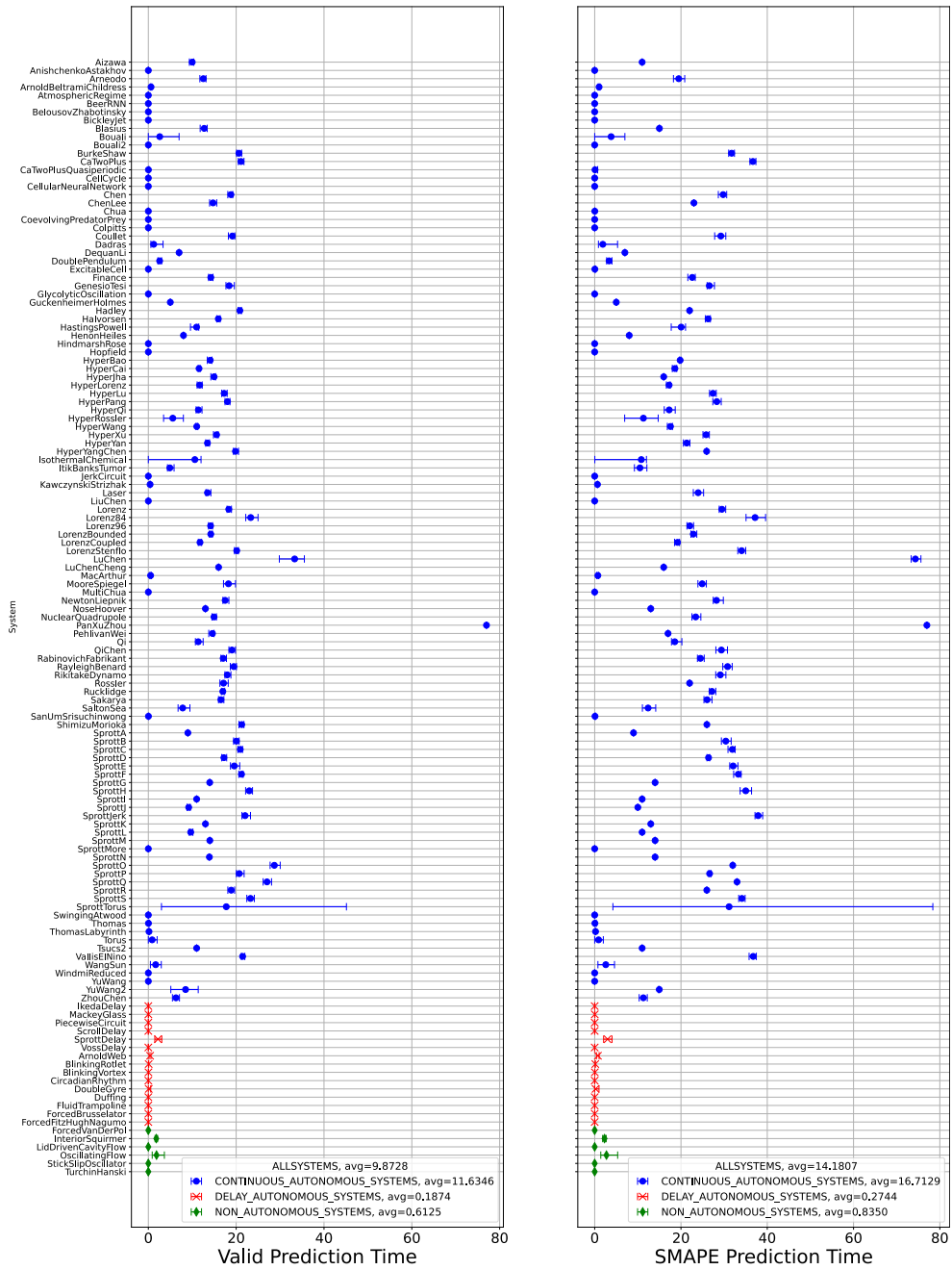


Fig. S5 Results evaluated using the same metrics and format as Fig. S1, but with different time steps: $T_{\text{warmup}} = 1000$ steps and $T_{\text{train}} = 2000$ steps.

References

- [1] Lorenz, E.N.: Deterministic nonperiodic flow. *J. Atmos. Sci.* **20**(2), 130–141 (1963)
- [2] May, R.M.: Simple mathematical models with very complicated dynamics. *Nature* **261**(5560), 459–467 (1976)
- [3] Mikhaeil, J.M., Monfared, Z., Durstewitz, D.: On the difficulty of learning chaotic dynamics with RNNs. *Neural Inf Process Syst* **35**, 11297–11312 (2021)
- [4] Vlachas, P.R., Byeon, W., Wan, Z.Y., Sapsis, T.P., Koumoutsakos, P.: Data-driven forecasting of high-dimensional chaotic systems with long short-term memory networks. *Proc. Math. Phys. Eng. Sci.* **474**(2213), 20170844 (2018)
- [5] Chattopadhyay, A., Hassanzadeh, P., Subramanian, D.: Data-driven predictions of a multiscale lorenz 96 chaotic system using machine-learning methods: reservoir computing, artificial neural network, and long short-term memory network. *Nonlinear Process. Geophys.* **27**(3), 373–389 (2020)
- [6] Jaeger, H.: The “echo state” approach to analysing and training recurrent neural networks. GMD Technical Report (148) (2001)
- [7] Maass, W., Natschläger, T., Markram, H.: Real-time computing without stable states: a new framework for neural computation based on perturbations. *Neural Comput.* **14**(11), 2531–2560 (2002)
- [8] Pathak, J., Lu, Z., Hunt, B.R., Girvan, M., Ott, E.: Using machine learning to replicate chaotic attractors and calculate lyapunov exponents from data. *Chaos* **27**(12), 121102 (2017)
- [9] Lu, Z., Hunt, B.R., Ott, E.: Attractor reconstruction by machine learning. *Chaos* **28**(6), 061104 (2018)
- [10] Takens, F.: Detecting strange attractors in turbulence. In: Rand, D., Young, L.-S. (eds.) *Dynamical Systems and Turbulence*, Warwick 1980, pp. 366–381. Springer, Berlin, Heidelberg (1981)
- [11] Sauer, T., Yorke, J.A., Casdagli, M.: Embedology. *J. Stat. Phys.* **65**(3), 579–616 (1991)
- [12] Hart, A., Hook, J., Dawes, J.: Embedding and approximation theorems for echo state networks. *Neural Netw.* **128**, 234–247 (2020)
- [13] Grigoryeva, L., Hart, A., Ortega, J.-P.: Chaos on compact manifolds: Differentiable synchronizations beyond the takens theorem. *Phys Rev E* **103**(6-1), 062204 (2021)

- [14] Margazoglou, G., Magri, L.: Stability analysis of chaotic systems from data. *Nonlinear Dyn.* **111**(9), 8799–8819 (2023)
- [15] Sisodia, D., Jalan, S.: Dynamical analysis of a parameter-aware reservoir computer. *Phys. Rev. E.* **110**(3-1), 034211 (2024)
- [16] Platt, J.A., Penny, S.G., Smith, T.A., Chen, T.-C., Abarbanel, H.D.I.: Constraining chaos: Enforcing dynamical invariants in the training of reservoir computers. *Chaos* **33**(10), 103107 (2023)
- [17] Balas, M.J.: Active control of flexible systems. *J. Optim. Theory Appl.* **25**(3), 415–436 (1978)
- [18] Datta, B.N., Elhay, S., Ram, Y.M.: Orthogonality and partial pole assignment for the symmetric definite quadratic pencil. *Linear Algebra Appl.* **257**, 29–48 (1997)
- [19] Kailath, T.: *Linear systems* **156** (1980)
- [20] Saad, Y.: Projection and deflation method for partial pole assignment in linear state feedback. *IEEE Trans. Automat. Contr.* **33**(3), 290–297 (1988)
- [21] Varga, A.: A schur method for pole assignment. *IEEE Trans. Automat. Contr.* **26**(2), 517–519 (1981)
- [22] Sauer, T.D., Tempkin, J.A., Yorke, J.A.: Spurious lyapunov exponents in attractor reconstruction. *Phys. Rev. Lett.* **81**(20), 4341–4344 (1998)
- [23] Theiler, J.: Spurious dimension from correlation algorithms applied to limited time-series data. *Phys. Rev. A Gen. Phys.* **34**(3), 2427–2432 (1986)
- [24] Rössler, O.: An equation for continuous chaos. *Physics Letters A* **57**, 397–398 (1976)
- [25] Menck, P.J., Heitzig, J., Marwan, N., Kurths, J.: How basin stability complements the linear-stability paradigm. *Nat. Phys.* **9**(2), 89–92 (2013)
- [26] Vlachas, P.R., Pathak, J., Hunt, B.R., Sapsis, T.P., Girvan, M., Ott, E., Koumoutsakos, P.: Backpropagation algorithms and reservoir computing in recurrent neural networks for the forecasting of complex spatiotemporal dynamics. *Neural Netw.* **126**, 191–217 (2020)
- [27] Platt, J.A., Wong, A., Clark, R., Penny, S.G., Abarbanel, H.D.I.: Robust forecasting using predictive generalized synchronization in reservoir computing. *Chaos* **31**(12), 123118 (2021)
- [28] Bollt, E.: On explaining the surprising success of reservoir computing forecaster of chaos? the universal machine learning dynamical system with contrast to VAR and DMD. *Chaos* **31**(1), 013108 (2021)

- [29] Hurley, L.A., Shaheen, S.E.: Reservoir computing with large valid prediction time for the lorenz system. arXiv [cs.NE] (2025) [cs.NE]
- [30] Fujisaka, H., Yamada, T.: Stability theory of synchronized motion in coupled-oscillator systems. Prog Theor Phys **69**(1), 32–47 (1983)
- [31] Kantz, H., Olbrich, E.: Scalar observations from a class of high-dimensional chaotic systems: Limitations of the time delay embedding. Chaos **7**(3), 423–429 (1997)
- [32] Pecora, L., Carroll, T.: Statistics for differential topological properties between datasets with an application to reservoir computers. Chaos **35**(7), 073153 (2025)
- [33] Kaplan, J.L., Yorke, J.A.: Chaotic behavior of multidimensional difference equations. In: Functional Differential Equations and Approximation of Fixed Points. Lecture notes in mathematics, pp. 204–227. Springer, Berlin, Heidelberg (1979)
- [34] Gilpin, W.: Chaos as an interpretable benchmark for forecasting and data-driven modelling. arXiv [cs.LG] (2021) [cs.LG]
- [35] Gilpin, W.: Model scale versus domain knowledge in statistical forecasting of chaotic systems. Phys. Rev. Res. **5**(4), 043252 (2023)
- [36] Oreshkin, B.N., Carpov, D., Chapados, N., Bengio, Y.: N-BEATS: Neural basis expansion analysis for interpretable time series forecasting. In: International Conference on Learning Representations (2020)
- [37] Challu, C., Olivares, K.G., Oreshkin, B.N., Garza, F., Mergenthaler-Canseco, M., Dubrawski, A.: N-HiTS: Neural hierarchical interpolation for time series forecasting. National Conference on Artificial Intelligence **abs/2201.12886** (2022)
- [38] Jaeger, H., Lukosevicius, M., Popovici, D., Siewert, U.: Optimization and applications of echo state networks with leaky-integrator neurons. Neural Netw. **20**(3), 335–352 (2007)
- [39] Tanaka, G., Yamane, T., Héroux, J.B., Nakane, R., Kanazawa, N., Takeda, S., Numata, H., Nakano, D., Hirose, A.: Recent advances in physical reservoir computing: A review. Neural Netw. **115**, 100–123 (2019)
- [40] Van Overschee, P., De Moor, B.: N4SID: Subspace algorithms for the identification of combined deterministic-stochastic systems. Automatica (1994)
- [41] Van Overschee, P., De Moor, B.: A unifying theorem for three subspace system identification algorithms. Automatica (Oxf.) **31**(12), 1853–1864 (1995)

- [42] Verhaegen, M.: Application of a subspace model identification technique to identify LTI systems operating in closed-loop. *Automatica (Oxf.)* **29**(4), 1027–1040 (1993)
- [43] Qin, S.J.: An overview of subspace identification. *Comput. Chem. Eng.* **30**(10-12), 1502–1513 (2006)
- [44] Schmid, P.J.: Dynamic mode decomposition of numerical and experimental data. *J. Fluid Mech.* **656**, 5–28 (2010)
- [45] Kutz, J.N., Brunton, S.L., Brunton, B.W., Proctor, J.L.: *Dynamic Mode Decomposition: Data-driven Modeling of Complex Systems*. SIAM, ??? (2016)
- [46] Grigoryeva, L., Hart, A., Ortega, J.-P.: Learning strange attractors with reservoir systems. *Nonlinearity* **36**(9), 4674 (2023)
- [47] Sussillo, D., Abbott, L.F.: Generating coherent patterns of activity from chaotic neural networks. *Neuron* **63**(4), 544–557 (2009)
- [48] Huang, G.-B., Zhu, Q.-Y., Siew, C.-K.: Extreme learning machine: Theory and applications. *Neurocomputing* **70**(1-3), 489–501 (2006)
- [49] Jaeger, H.: Echo state network. *Scholarpedia* **2**(9), 2330 (2007)
- [50] Lukoševičius, M., Jaeger, H.: Reservoir computing approaches to recurrent neural network training. *Comput. Sci. Rev.* **3**(3), 127–149 (2009)
- [51] Rulkov, N.F., Sushchik, M.M., Tsimring, L.S., Abarbanel, H.D.: Generalized synchronization of chaos in directionally coupled chaotic systems. *Phys. Rev. E Stat. Phys. Plasmas Fluids Relat. Interdiscip. Topics* **51**(2), 980–994 (1995)
- [52] Kocarev, L., Parlitz, U.: Generalized synchronization, predictability, and equivalence of unidirectionally coupled dynamical systems. *Phys. Rev. Lett.* **76**(11), 1816–1819 (1996)
- [53] Hunt, B.R., Ott, E., Yorke, J.A.: Differentiable generalized synchronization of chaos. *Phys. Rev. E Stat. Phys. Plasmas Fluids Relat. Interdiscip. Topics* **55**(4), 4029–4034 (1997)
- [54] Flynn, A., Tsachouridis, V.A., Amann, A.: Multifunctionality in a reservoir computer. *Chaos* **31**(1), 013125 (2021)
- [55] O’Hagan, J., Keane, A., Flynn, A.: Confabulation dynamics in a reservoir computer: Filling in the gaps with untrained attractors. *Chaos* **35**(9), 093130 (2025)
- [56] Hart, J.D.: Attractor reconstruction with reservoir computers: The effect of the reservoir’s conditional lyapunov exponents on faithful attractor reconstruction.

Chaos **34**(4), 043123 (2024)

- [57] Shimada, I., Nagashima, T.: A numerical approach to ergodic problem of dissipative dynamical systems. *Prog. Theor. Phys.* **61**(6), 1605–1616 (1979)
- [58] Benettin, G., Galgani, L., Giorgilli, A., Strelcyn, J.-M.: Lyapunov characteristic exponents for smooth dynamical systems and for hamiltonian systems; a method for computing all of them. part 2: Numerical application. *Meccanica* **15**(1), 21–30 (1980)